$MAPbI_3$ 钙钛矿纳米线光电探测器

刘艳珍，崔艳霞*

太原理工大学物理与光电工程学院，新型传感与智能控制教育部重点实验室，山西 太原 030024

摘要 有机-无机杂化钙钛矿纳米材料因其具有直接带隙、吸收系数高、载流子迁移率高等特点成为新一代优良的光电探测材料。诸多研究表明该纳米材料具有量子点、纳米线、纳米棒、纳米片等多种形貌。纳米线结构具有各向异性，光生载流子沿其轴向高效传输，有利于改善光电探测器的电荷提取效率。基于此，采用自组装生长法制备了钙钛矿纳米线阵列，当前驱体溶液质量分数从 10%逐渐减小为 0.2%时，纳米线直径从微米量级减小至百纳米量级。将 0.5%的前驱体溶液所得的纳米线阵列应用到光电探测器中，器件在 2 V 偏压、660 nm 红光照射下亮暗电流比高达 3.7×10^4，外量子效率高达 180.88%，而暗电流密度低至 1 pA。器件光电探测性能的显著改善归功于自组装生长的纳米线在径向的均匀排布及其高结晶质量。

关键词 光学器件；钙钛矿；纳米线；光电探测器

中图分类号 O472 **文献标识码** A **doi**：10.3788/LOP55.102301

$MAPbI_3$ Perovskite Nanowire Photodetectors

Liu Yanzhen, Cui Yanxia*

Key Laboratory of Advanced Transducers and Intelligent Control System, Ministry of Education, College of Physics and Optoelectronics, Taiyuan University of Technology, Taiyuan, Shanxi 030024, *China*

Abstract Organic-inorganic hybrid perovskite is a promising new generation of photodetection materials due to its advantages of direct bandgap, high absorption coefficient, and high carrier mobility. Researches have shown that the perovskite nanomaterials have various morphologies, such as quantum dots, nanowires, nanorods, and nanosheets. In particular the anisotropic nanowires photogenerated carriers transmit efficiently along the axial direction, which enhances the charge extraction efficiency of the photodetector. In this paper, the perovskite nanowire arrays were prepared by the self-assembly growth method. When the mass fraction of precursor solution decreased from 10% to 0.2%, the diameter of nanowires was reduced from micron to hundred nanometer scale. A photodetector based on nanowire arrays obtained from 0.5% precursor solution was reported. The light-to-dark response ratio of the device was as high as 3.7×10^4, the external quantum efficiency reached up to 180.88%, and the dark current density was as low as 1 pA. All data were measured under 2 V bias voltage and 660 nm red light. The remarkable improvement of the photodetector performance is attributed to the radial uniform distribution of the nanowires and high crystallization quality.

Key words optical devices; perovskite; nanowires; photodetector

OCIS codes 230.5160; 160.6000

1 引 言

基于钙钛矿材料的光伏电池已实现 20%以上的光电转换效率，接近商用的硅基电池，成为研究者们关注的新一代半导体材料[1-3]。钙钛矿材料是直接带隙材料，具有从可见光到近红外波段的宽吸收光谱[1,4-9]，吸光系数高，为其高光电转换效率奠定了基础。钙钛矿单晶晶体具有极低的缺陷态密度(10^8 cm^{-3})[10]，在实现弱光探测方面具有很大的应用潜力[8]。随着制备工艺的多样化，钙钛矿材料的

收稿日期：2018-04-23；**修回日期**：2018-05-22；**录用日期**：2018-05-25

基金项目：国家自然科学基金(61775156，61475109，61605136)、山西省自然科学基金优秀青年科学基金(201701D211002)、山西省重点研发(国际合作)项目(201603D421042)、山西省青年拔尖人才资助项目、青年三晋学者基金

* **E-mail**：yanxiacui@gmail.com

结晶形貌越来越丰富，从最初旋涂制备的微晶/多晶薄膜[11-16]，到饱和结晶法得到的厘米级大小的单晶[10,17-25]，以及气相或液相合成的低维纳米单晶[4,10,26-38]。其中低维纳米单晶又包括零维量子点、纳米颗粒、一维纳米线与二维纳米片等。纳米线在轴向与径向呈现光学各向异性，可检测光的偏振[27]；长光程在纳米线的轴向，可实现高的光吸收；载流子传输方向受到线结构束缚，沿着轴向，减少了可能的激子传输损耗。此外，钙钛矿纳米线具有优异的力学稳定性，可制成柔性器件，阵列形貌的纳米线结构还便于微纳米光电子器件的集成应用[29-30,32]。

目前，钙钛矿纳米线阵列结构的制备是科学家们研究的热点，其制备方法有：模板限制生长法——利用阳极氧化铝(AAO)阵列纳米孔模板限制晶体在纳米孔中生长成纳米线，或者利用阵列凹凸微观结构模板结合饱和溶液结晶生长钙钛矿纳米线阵列[29,38-39]；刮涂生长——利用刮涂提供液体干燥方向即纳米线生长方向[30]；倾斜衬底自组装生长——在倾斜的衬底上滴涂前驱体溶液，液体自然随着流动方向形成干燥速度差，饱和前驱体溶液挥发结晶形成纳米线阵列[27,32]。

本文利用倾斜衬底自组装生长了甲胺铅碘($MAPbI_3$)钙钛矿纳米线(NW)阵列，并且研究了前驱体溶液浓度对 $MAPbI_3$ NW 直径的影响。制备了基于 $MAPbI_3$ NW 的光电导探测器，表征探测器的响应速度、线性动态范围、外量子效率、响应率、探测率与稳定性等。

2 实验方法

利用倾斜衬底自组装的方法生长 $MAPbI_3$ NW。这种方法简单高效，在没有外力作用或模板的情况下制得阵列有序的 $MAPbI_3$ NW，并制备了基于 $MAPbI_3$ NW 的光电探测器。

药品来源：碘化铅(PbI_2，纯度 99.99%)与甲基碘化铵(MAI，纯度 99.5%)购自西安宝莱特，N,N-二甲基甲酰胺(DMF)购自 Sigma。

实验工艺如图 1 所示。具体步骤可分为溶液配制、纳米线生长与电极蒸镀三部分。

2.1 溶液配制

1) 配制 10%(质量分数)的 $MAPbI_3$(DMF)溶液：称量 MAI 0.05385 g，PbI_2 0.156 g，加入 2 mL DMF 即得，其中 DMF 的密度为 0.945 g/mL。

2) 使用常温振荡溶解钙钛矿溶液，不能加热与搅拌，振荡十几秒，使溶液变清亮，之后静置一段时间再使用。

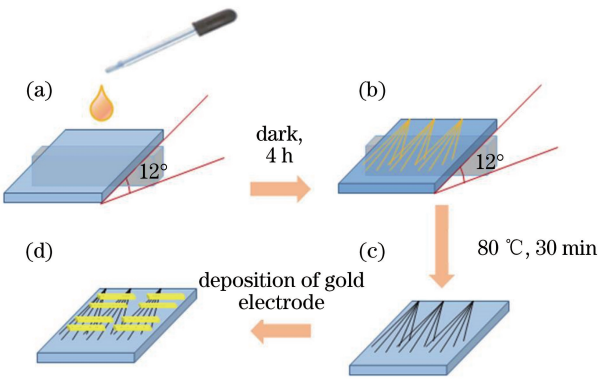

图 1 自组装法生长 $MAPbI_3$ NW 实验过程。(a)在 12°斜坡上滴涂前驱体溶液；(b)暗态下静置 4 h，纳米线成型；(c) 80 ℃加热 30 min，生成钙钛矿纳米线；(d)真空热沉积金属电极，制备 $MAPbI_3$ NW 光电探测器

Fig. 1 Schematic of the growing process of $MAPbI_3$ NWs by self-assembly growth method. (a) Drip the precursor solution on a glass with 12° slope; (b) place the substrate in a dark state for 4 h to grow nanowires; (c) heat at 80 ℃ for 30 min to generate $MAPbI_3$ NWs; (d) vacuum thermal deposition of metal electrodes to prepare $MAPbI_3$ NWs photodetectors

3) 配制质量分数更大的溶液需要重新计算称量配制，而质量分数低于 10%的溶液可以由该液稀释，之后振荡使溶液混合均匀。配制 5%的溶液：取 500 μL 10%溶液，再加入 611 μL DMF；配制 2%溶液：取 400 μL 10%溶液，再加入 1.82 mL DMF；配制 1%溶液：取 400 μL 10%溶液，再加入 3.9 mL DMF；配制 0.5%溶液：取 500 μL 1%溶液，再加入 611 μL DMF；配制 0.2%溶液：取 400 μL 1%溶液，再加入 1.82 mL DMF。

2.2 玻璃衬底上生长 $MAPbI_3$ NW

1) 用洗洁精搓洗玻璃衬底(1 cm×1 cm)，然后分别用去离子水、乙醇、异丙醇超声清洗玻璃衬底，之后烘干，等离子清洗机处理 5 min。

2) 将玻璃衬底放在倾斜 12°的斜坡上，用 10 μL 移液枪分别取 0.2%、0.5%、2%、5%与 10%的前驱体溶液 3 μL 滴涂在衬底上，溶液瞬间铺展。

3) 盖住衬底，在干燥、黑暗、室温、空气环境下静置约 4 h，等待纳米线生长。

4) 纳米线缓慢生长成型后，在 80 ℃的加热台上加热 30 min，转变成钙钛矿纳米线。

2.3 真空热蒸镀金电极

利用沈阳立宁真空技术研究所生产的 LN-1084SC 型真空镀膜机制备金电极。所用掩模板为栅

条形状的铜网，蒸镀压强约为 5×10^{-4} Pa，蒸镀速率为 0.2 nm/s，金电极厚度为 70 nm，电极间距为 41.82 μm，器件有效面积为 1.25×10^{-3} cm^2[图 2(f)]。

3 实验结果

首先对不同质量分数的前驱体溶液制得的 $MAPbI_3$ NW 进行表征。图 2 为对应不同质量分数的溶液制备的 $MAPbI_3$ NW 光学显微图，随着溶液质量分数的增大，纳米线的直径增加，0.2%溶液纳米线直径 0.55 μm 左右，0.5%溶液纳米线直径 0.86 μm 左右，2%溶液纳米线直径 1 μm 左右，5%溶液纳米线直径 1.4 μm 左右，10%溶液纳米线直径 3.27 μm 左右。

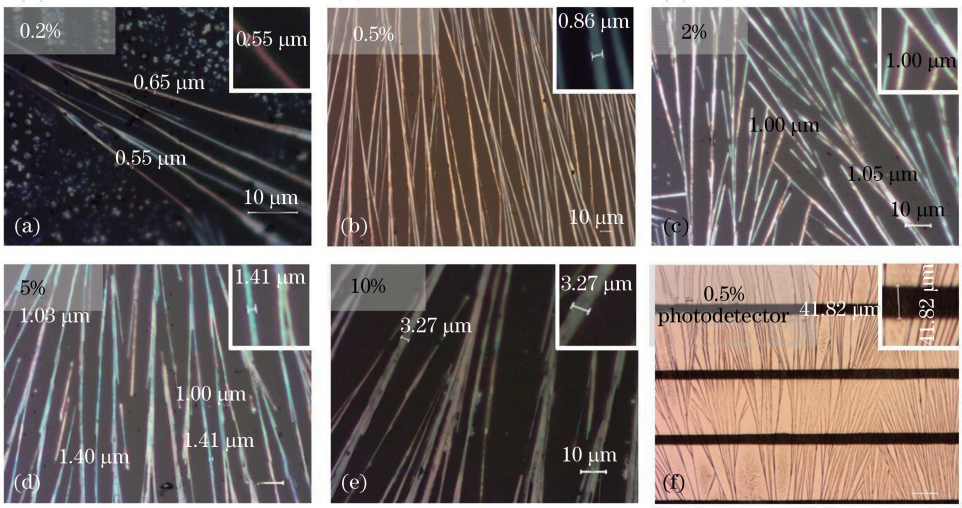

图 2 (a)～(e)不同质量分数前驱体溶液生成的 $MAPbI_3$ NW 光学显微图；(f) $MAPbI_3$ NW 探测器光学显微图

Fig. 2 (a)-(e) Optical micrographs of $MAPbI_3$ NWs generated from different concentrations of precursor solution; (f) optical micrograph of $MAPbI_3$ NWs photodetector

图 3 表征了 $MAPbI_3$ NW 的紫外可见吸收光谱、光致发光(PL)谱与 X 射线衍射(XRD)谱。图中对比了不同质量分数前驱体溶液生长的 $MAPbI_3$ NW 的紫外可见吸收光谱与 PL 谱，随着前驱体溶液质量分数增大，$MAPbI_3$ NW 吸收增强，PL 增强。在 325 nm、1 mW激光照射下的 PL 谱半峰全宽(FWHM)分别为 37 nm (0.2%)、38 nm (0.5%)、34 nm (2%)、36 nm (5%)和 40 nm (10%)，峰值位置在 766 nm。$MAPbI_3$ NW 的 XRD 谱如图 3(c)所示，对应了正方结构的钙钛矿材料[2,40]。

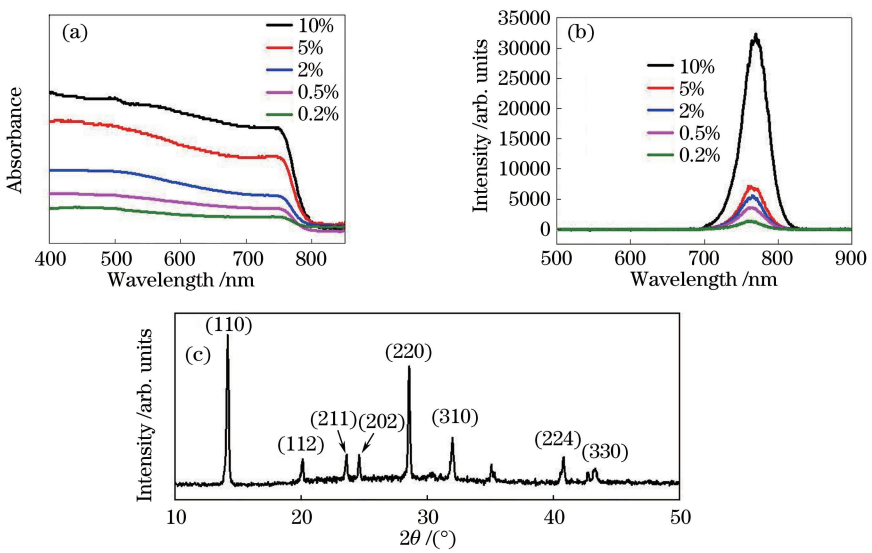

图 3 不同浓度前驱体溶液生长的 $MAPbI_3$ NW (a)紫外可见吸收光谱与(b) PL 谱；(c) $MAPbI_3$ NW 的 XRD 谱

Fig. 3 (a) UV-visible absorbtion spectra and (b) PL spectra of $MAPbI_3$ NWs generated from different concentrations of precursor solution; (c) XRD pattern of $MAPbI_3$ NWs

选取0.5%前驱体溶液生长的$MAPbI_3$ NW制备光电导型探测器[图2(f)]。半导体分析仪Agilent B1500A、红色LED(Thorlabs,波长660 nm)光源用来测试$MAPbI_3$ NW光电探测器的性能。图4(a)表征了器件的电流-电压曲线,曲线斜率随光照强度增大而增大,值得注意的是,暗态下电流强度为1 pA量级。

光电探测器的一个重要指标是亮暗电流比,顾名思义,是指光照情况下电流与黑暗情况下电流的比值,这个值越大越好。在图4(b)中将图4(a)所示暗态与入射光功率密度105.1 mW/cm^{2}下的电流值取对数,由图可知器件的亮暗电流比为3.7×10^4。图4(c)表征$MAPbI_3$ NW光电探测器在周期为10 s的方波脉冲LED(660 nm)光照下的响应。探测器的电流随光照的亮暗呈周期性同步增大或减小,且其幅值保持稳定。

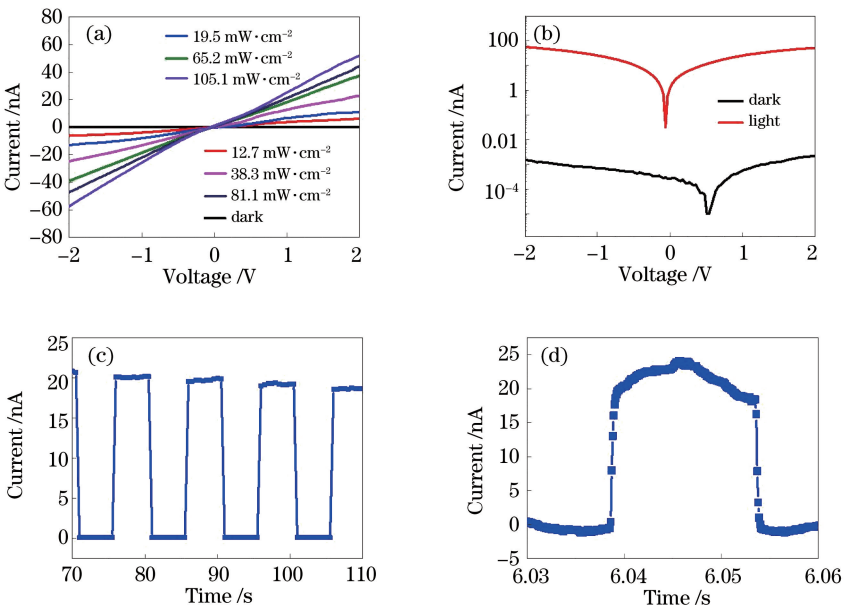

图4 (a) $MAPbI_3$ NW光电探测器在不同入射光强下的电流-电压曲线;(b) $MAPbI_3$ NW光电探测器在暗态与105.1 mW/cm^2 LED(660 nm)照射下的对数电流-电压曲线;(c) $MAPbI_3$ NW光电探测器在周期为10 s的方波LED(660 nm)光照下的响应;(d)光电探测器的响应速度

Fig. 4 (a) Current-voltage curves of $MAPbI_3$ NWs photodetector under different incident light intensity; (b) current-voltage curves of $MAPbI_3$ NWs photodetector with logarithmic coordinate in the dark state and 105.1 mW/cm^2 LED (660 nm) irradiation; (c) $MAPbI_3$ NWs photodetector response to a periodic LED (660 nm) illumination with a period of 10 s; (d) response time of $MAPbI_3$ NWs photodetector

光电探测器的响应速度由光照射瞬间响应电流从10%上升到90%所用时间,以及光照关闭瞬间光电流从90%下降到10%所用时间表示,这两个时间分别定义为上升沿时间与下降沿时间。图4(d)为LED(660 nm)光源以30 ms的周期呈现亮暗变化的情形下,测得的$MAPbI_3$ NW光电探测器电流随时间的响应,响应速度上升沿与下降沿时间均为0.3 ms。

线性动态范围(r_{LDR})是指光电流随着入射光功率密度呈线性变化的区间,数值计算公式为

$$r_{LDR}=20\log\frac{P_{sat}}{P_{low}},\qquad(1)$$

式中:P_{sat}与P_{low}分别代表光电流达到饱和时的入射光功率密度与偏离线性区域的最低光电流对应的入射光功率密度。图5(a)为器件r_{LDR}测试曲线,电流随光强变化的线性区域对应的入射光功率密度为0.0056~105 mW/cm^2,按照(1)式计算得r_{LDR}为86.3 dB。图中暗电流按线性延升直线得到一个理想的最大r_{LDR},对应的入射光功率密度为7.44×10^{-4}~105 mW/cm^2,按照(1)式计算得到理想r_{LDR}为103 dB。图中器件光电流还未达到饱和,但是光源的光强值限制了对r_{LDR}的测试表征。

有关光电探测器的其他表征参数为响应率(R)、探测率(D^*)以及外量子效率(η_{EQE})。响应率为光电流密度I_{ph}与入射光功率密度P_{in}之比,表征探测器对入射光的响应能力。探测率表示光电探测器的探测能力,其值越大越好。η_{EQE}为光电探测器中每秒内产生的光电子数与入射光量子数之比,η_{EQE}越高越好。几个参数的表达式为

$$R=\frac{I_{ph}}{P_{in}}, \tag{2}$$

$$D^{*}=\frac{R}{\sqrt{2eJ_{d}}}, \tag{3}$$

$$\eta_{EQE}=\frac{I_{ph}/e}{P_{in}/h\nu}, \tag{4}$$

式中：e 为单位电荷；J_d 为暗电流密度；h 为普朗克常量；ν 为入射光频率。

图 5(b)为 $MAPbI_3$ NW 光电探测器的响应率与探测率曲线，图 5(c)为其外量子效率曲线。随着入射光功率密度的增大，$MAPbI_3$ NW 光电探测器的响应率、探测率以及外量子效率均呈现减小趋势。当测试条件为 2 V 偏压、LED (660 nm)光功率密度为0.00816 mW/cm^{2}时，响应率最高为 0.96 mA/W，探测率最高为 5.31×10^{10} Jones。由于存在光电导增益，器件的外量子效率高于 100%，在 2 V 偏压、0.00816 mW/cm^{2}时达到最高值 180.88%。当入射光功率密度继续减小，响应率、探测率与外量子效率数值会相应增大。图 5(d)表征了未经封装等特殊手段处理的 $MAPbI_3$ NW 光电探测器在 20 ℃、相对湿度 50%的空气环境下的稳定性。测试条件恒为 2 V 偏压，LED (660 nm)光功率密度为105 mW/cm^2。由图可见器件的光电流在 7 d 内下降了 40%，稳定性还有待提高。目前，研究者们也提出了一系列封装、钝化钙钛矿光电子器件的手段[27,41-45]，本研究可以依此作进一步优化，提高稳定性。

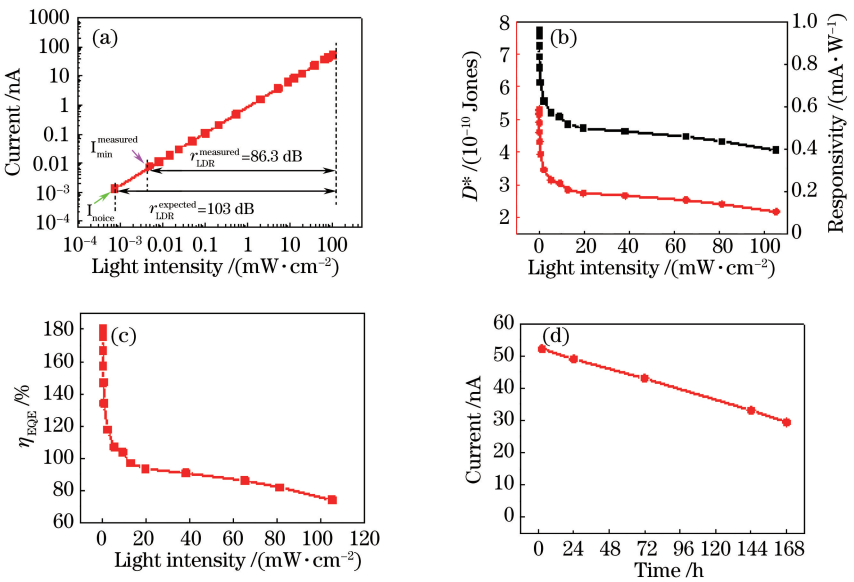

图 5 $MAPbI_3$ NW 光电探测器性能表征。(a)线性动态范围曲线；(b)响应率与探测率曲线；(c)外量子效率曲线；(d)稳定性测试曲线

Fig. 5 Performance characterization of $MAPbI_3$ NWs photodetector. (a) Linear dynanic range curve; (b) responsivity and detectivity curves; (c) external quantum efficiency curve; (d) stability test curve

4 结 论

研究了前驱体溶液质量分数对阵列 $MAPbI_3$ NW 直径的影响，基于 0.2%、0.5%、2%、5%、10%的溶液分别制得直径约为 0.55，0.86，1，1.4，3.27 μm的阵列 $MAPbI_3$ NW。表征了由 0.5%前驱体溶液制得的阵列 $MAPbI_3$ NW 光电导探测器的相关性能，器件的亮暗电流比高达 3.7×10^4，外量子效率高达 180.88%。响应速度上升沿与下降沿时间均为 0.3 ms，线性动态范围为 103 dB，响应率为 0.96 mA/W，探测率为 5.31×10^{10} Jones。该光电探测器在空气环境下储存 7 d，光电流下降了 40%，通过封装与钝化等方法可以进一步提高器件的稳定性。本文所述阵列形貌的 $MAPbI_3$ NW 可制成光电探测器阵列，在大面积、高像素点的图像传感器领域具有光明的应用前景。

致谢 感谢华中科技大学宋海胜教授与他的学生邓辉、董东冬对本工作的指导。

参 考 文 献

[1] Miller E M, Zhao Y, Mercado C C, *et al*. Substrate-controlled band positions in $CH_3NH_3PbI_3$ perovskite films [J]. Physical Chemistry Chemical Physics, 2014, 16(40): 22122-22130.

[2] Docampo P, Ball J M, Darwich M, *et al*. Efficient

organometal trihalide perovskite planar-heterojunction solar cells on flexible polymer substrates[J]. Nature Communications, 2013, 4(7): 2761.

[3] Shi X, Sun C, Wang X Q. One-dimensional diffraction grating structure for rear reflection surface of thin film silicon solar cells [J]. Laser & Optoelectronics Progress, 2018, 55(1): 010501.
石鑫, 孙诚, 王晓秋. 适用于薄膜硅太阳能电池背反射面的一维衍射光栅结构[J]. 激光与光电子学进展, 2018, 55(1): 010501.

[4] Ramasamy P, Lim D H, Kim B, *et al*. All-inorganic cesium lead halide perovskite nanocrystals for photodetector applications [J]. Chemical Communications, 2016, 52(10): 2067-2070.

[5] Dong D, Deng H, Hu C, *et al*. Bandgap tunable $Cs_x(CH_3NH_3)_{1-x}PbI_3$ perovskite nanowires by aqueous solution synthesis for optoelectronic devices [J]. Nanoscale, 2017, 9(4): 1567-1574.

[6] Wu X Y, Xiong Z Y, Wu L Y, *et al*. Enhancing perovskite fluorescence emission by gold nanoparticles[J]. Acta Optica Sinica, 2017, 37(9): 0924001.
吴小龑, 熊自阳, 吴凌远, 等. 金纳米粒子增强钙钛矿的荧光发射[J]. 光学学报, 2017, 37(9): 0924001.

[7] Bekenstein Y, Koscher B A, Eaton S W, *et al*. Highly luminescent colloidal nanoplates of perovskite cesium lead halide and their oriented assemblies[J]. Journal of the American Chemical Society, 2015, 137(51): 16008-16011.

[8] Fang Y, Dong Q, Shao Y, *et al*. Highly narrowband perovskite single-crystal photodetectors enabled by surface-charge recombination[J]. Nature Photonics, 2015, 9(10): 679-686.

[9] Filip M R, Eperon G E, Snaith H J, *et al*. Steric engineering of metal-halide perovskites with tunable optical band gaps [J]. Nature Communications, 2014, 5: 5757.

[10] Lian Z, Yan Q, Lv Q, *et al*. High-performance planar-type photodetector on (100) facet of $MAPbI_3$ single crystal [J]. Scientific Reports, 2015, 5: 16563.

[11] Hu X, Zhang X, Liang L, *et al*. High-performance flexible broadband photodetector based on organolead halide perovskite[J]. Advanced Functional Materials, 2014, 24(46): 7373-7380.

[12] Xia H R, Li J, Sun W T, *et al*. Organohalide lead perovskite based photodetectors with much enhanced performance[J]. Chemical Communications, 2014, 50(89): 13695-13697.

[13] Zhang Y, Du J, Wu X, *et al*. Ultrasensitive photodetectors based on island-structured $CH_3NH_3PbI_3$ thin films[J]. ACS Applied Materials & Interfaces, 2015, 7(39): 21634-21638.

[14] Liu C, Wang K, Du P, *et al*. Ultrasensitive solution-processed broad-band photodetectors using $CH_3NH_3PbI_3$ perovskite hybrids and PbS quantum dots as light harvesters[J]. Nanoscale, 2015, 7(39): 16460-16469.

[15] Liu C, Wang K, Yi C, *et al*. Ultrasensitive solution-processed perovskite hybrid photodetectors [J]. Journal of Materials Chemistry C, 2015, 3(26): 6600-6606.

[16] Zhao F Y, Xu K, Luo X, *et al*. Ultrasensitivity broadband photodetectors based on perovskite: research on film crystallization and electrode optimization[J]. Organic Electronics, 2017, 46: 35-43.

[17] Liu Y, Sun J, Yang Z, *et al*. 20-mm-large single-crystalline formamidinium-perovskite wafer for mass production of integrated photodetectors [J]. Advanced Optical Materials, 2016, 4(11): 1829-1837.

[18] Sun Z H, Zeb A R, Liu S J, *et al*. Exploring a lead-free semiconducting hybrid ferroelectric with a zero-dimensional perovskite-like structure [J]. Angewandte Chemie - International Edition, 2016, 55(39): 11854-11858.

[19] Zhang Y, Liu Y, Li Y, *et al*. Perovskite $CH_3NH_3Pb(Br_xI_{1-x})_3$ single crystals with controlled composition for fine-tuned bandgap towards optimized optoelectronic applications[J]. Journal of Materials Chemistry C, 2016, 4(39): 9172-9178.

[20] Fang H, Li Q, Ding J, *et al*. A self-powered organolead halide perovskite single crystal photodetector driven by a DVD-based triboelectric nanogenerator[J]. Journal of Materials Chemistry C, 2016, 4(3): 630-636.

[21] Ding J, Fang H, Lian Z, *et al*. A self-powered photodetector based on a $CH_3NH_3PbI_3$ single crystal with asymmetric electrodes [J]. CrystEngComm, 2016, 18(23): 4405-4411.

[22] Lin Q, Armin A, Burn P L, *et al*. Near infrared photodetectors based on sub-gap absorption in organohalide perovskite single crystals[J]. Laser & Photonics Reviews, 2016, 10(6): 1047-1053.

[23] Shewmon N T, Yu H, Constantinou I, *et al*. Formation of perovskite heterostructures by ion exchange[J]. ACS Applied Materials & Interfaces, 2016, 8(48): 33273-33279.

[24] Liu Y, Zhang Y, Yang Z, *et al*. Thinness- and shape-controlled growth for ultrathin single-crystalline perovskite wafers for mass production of superior photoelectronic devices [J]. Advanced Materials, 2016, 28(41): 9204-9209.

[25] Han Q, Bae S-H, Sun P, *et al*. Single crystal formamidinium lead iodide ($FAPbI_3$): insight into the structural, optical, and electrical properties[J]. Advanced Materials, 2016, 28(11): 2253-2258.

[26] Huo C X, Wang Z M, Li X M, *et al*. Low-dimensional metal halide perovskites: a kind of microcavity laser materials[J]. Chinese Journal of Lasers, 2017, 44(7): 0703008.
霍成学, 王子明, 李晓明, 等. 低维金属卤化物钙钛矿: 一种微腔激光材料[J]. 中国激光, 2017, 44(7): 0703008.

[27] Gao L, Zeng K, Guo J, *et al*. Passivated single-crystalline $CH_3NH_3PbI_3$ nanowire photodetector with high detectivity and polarization sensitivity[J]. Nano Letters, 2016, 16(12): 7446-7454.

[28] Zhuo S, Zhang J, Shi Y, *et al*. Self-template-directed synthesis of porous perovskite nanowires at room temperature for high-performance visible-light photodetectors [J]. Angewandte Chemie - International Edition, 2015, 54(19): 5693-5696.

[29] Deng W, Huang L, Xu X, *et al*. Ultrahigh-responsivity photodetectors from perovskite nanowire arrays for sequentially tunable spectral measurement [J]. Nano Letters, 2017, 17(4): 2482-2489.

[30] Deng W, Zhang X, Huang L, *et al*. Aligned single-crystalline perovskite microwire arrays for high-performance flexible image sensors with long-term stability[J]. Advanced Materials, 2016, 28(11): 2201-2208.

[31] Horvath E, Spina M, Szekrenyes Z, *et al*. Nanowires of methylammonium lead iodide ($CH_3NH_3PbI_3$) prepared by low temperature solution-mediated crystallization[J]. Nano Letters, 2014, 14(12): 6761-6766.

[32] Deng H, Dong D, Qiao K, *et al*. Growth, patterning and alignment of organolead iodide perovskite nanowires for optoelectronic devices[J]. Nanoscale, 2015, 7(9): 4163-4170.

[33] Gao T, Zhang Q, Chen J N, *et al*. Performance-enhancing broadband and flexible photodetectors based on perovskite/ZnO-nanowire hybrid structures [J]. Advanced Optical Materials, 2017, 5(12): 1700206.

[34] Niu L, Zeng Q, Shi J, *et al*. Controlled growth and reliable thickness-dependent properties of organic-inorganic perovskite platelet crystal[J]. Advanced Functional Materials, 2016, 26(29): 5263-5270.

[35] Liu X H, Yu D J, Cao F, *et al*. Low-voltage photodetectors with high responsivity based on solution-processed micrometer-scale all-inorganic perovskite nanoplatelets[J]. Small, 2017, 13(25): 1700364.

[36] Song J, Xu L, Li J, *et al*. Monolayer and few-layer all-inorganic perovskites as a new family of two-dimensional semiconductors for printable optoelectronic devices [J]. Advanced Materials, 2016, 28(24): 4861-4869.

[37] Qin X, Yao Y, Dong H, *et al*. Perovskite photodetectors based on $CH_3NH_3PbI_3$ single crystals [J]. Chemistry - An Asian Journal, 2016, 11(19): 2675-2679.

[38] Tan Z, Wu Y, Hong H, *et al*. Two-dimensional $(C_4H_9NH_3)_2PbBr_4$ perovskite crystals for high-performance photodetector [J]. Journal of the American Chemical Society, 2016, 138(51): 16612-16615.

[39] Hu Q, Wu H, Sun J, *et al*. Large-area perovskite nanowire arrays fabricated by large-scale roll-to-roll micro-gravure printing and doctor blading [J]. Nanoscale, 2016, 8(9): 5350-5357.

[40] Ashley M J, O'Brien M N, Hedderick K R, *et al*. Templated synthesis of uniform perovskite nanowire arrays [J]. Journal of the American Chemical Society, 2016, 138(32): 10096-10099.

[41] You J, Meng L, Song T-B, *et al*. Improved air stability of perovskite solar cells via solution-processed metal oxide transport layers[J]. Nature Nanotechnology, 2016, 11(1): 75-81.

[42] Kwon K C, Hong K, Van Le Q, *et al*. Inhibition of ion migration for reliable operation of organolead halide perovskite-based metal/semiconductor/metal broadband photodetectors[J]. Advanced Functional Materials, 2016, 26(23): 4213-4222.

[43] Guo Y, Liu C, Tanaka H, *et al*. Air-stable and solution-processable perovskite photodetectors for solar-blind UV and visible light [J]. Journal of Physical Chemistry Letters, 2015, 6(3): 535-539.

[44] Slayney A H, Smaha R W, Smith I C, *et al*. Chemical approaches to addressing the instability and toxicity of lead-halide perovskite absorbers [J]. Inorganic Chemistry, 2017, 56(1): 46-55.

[45] Waleed A, Tavakoli M M, Gu L, *et al*. Lead-free perovskite nanowire array photodetectors with drastically improved stability in nanoengineering templates[J]. Nano Letters, 2017, 17(1): 523-530.